



Formulation of turbulence diffusion relationships under stable atmospheric conditions and its effect on pollution dispersion

P. T. Rakesh¹ · R. Venkatesan¹ · P. Roubin² · C. V. Srinivas¹ · R. Baskaran¹ · B. Venkatraman¹

Received: 30 June 2019 / Accepted: 27 January 2020 / Published online: 10 February 2020
© Springer-Verlag GmbH Austria, part of Springer Nature 2020

Abstract

In this article, we formulate Monin–Obukhov similarity theory (MOST)-based relationships, for normalized standard deviations of wind velocity components under the local scaling framework, and investigate their applicability under stable and highly stable atmospheric conditions. We used the fast response data collected using an ultrasonic anemometer over a flat terrain of Kalpakkam in India and a complex hilly terrain at Cadarache, France, for arriving at these formulations. The study shows that after filtering of the submesoscale motions from the sonic anemometer data, the turbulence diffusion relationships follow local scaling, under stable conditions. The study further indicates that these relationships follow similar behavior for the sites taken for this study. At neutral conditions, the values of the scaled standard deviations are found to be 1.9 ± 0.07 , 1.8 ± 0.06 and 1.3 ± 0.02 , for longitudinal, crosswind and vertical component, respectively, for the complex terrain and 1.8 ± 0.03 , 1.9 ± 0.06 and 1.1 ± 0.04 , respectively, for the flat terrain. The research also investigates the effect of the new diffusion relationships in simulating atmospheric dispersion, using the Lagrangian particle dispersion model FLEXPART-WRF. Simulations using these new diffusion relationships show a higher dose estimate relative to the model default Hanna's method, in the case of radioactivity dispersion. Detailed comparisons of the simulated dose rate estimates against measurements using Environmental Radiation Monitors (ERM) indicate that the new relationships give better correlation ($r^2 = 0.62$) under stable conditions over model default relationships ($r^2 = 0.50$).

Keywords Monin–obukhov similarity theory · Local scaling · Multi-resolution decomposition · WRF · FLEXPART · Dispersion modeling

1 Introduction

The Monin–Obukhov similarity theory (MOST) (Monin and Obukhov 1954; Businger et al. 1971) is a widely used framework, to obtain turbulent fluxes in the atmospheric surface layer, as a function of the standard scaling variable such as friction velocity u_* , surface roughness z_0 , boundary layer height z_i , and Monin–Obukhov length L . Following the MOST, the turbulent fluxes of wind, temperature,

and moisture in the surface layer are related to the vertical gradients of their mean quantities by an eddy diffusivity coefficient, K_z (Garra 1994). Many boundary layer models use the MOST, for obtaining the mean meteorological variables in the lower turbulent layer and wind power meteorology (Businger and Arya 1974; Wyngaard 1975; Petersen et al. 1998; Lange and Focken 2005; Monteiro et al. 2009; Emeis 2010, 2013). However, under very stable atmospheric condition, the application of the MOST was not successful in representing the turbulence and the stability functions, realistically due to the sensitivity to frequently observed submesoscale phenomena-like gravity waves, meandering motions, radiative divergence, intermittency, etc. (Mahrt 1999; Mahrt and Vickers 2006; Vande Wiel et al. 2003; Mahrt 2011, 2014). The non-turbulent submesoscale motions are the horizontal fluctuations on the scale of 0.02–2 km (Metstayer and Anquetin 1995; Belusich and Mahrt 2008). Nieuwstadt (1984) introduced the local scaling, based on second-order closure equations using

Responsible Editor: S. Trini Castelli.

✉ P. T. Rakesh
rakeshpt@gmail.com

¹ Radiological Safety Division, Indira Gandhi Centre for Atomic Research, HBNI, Kalpakkam, Tamil Nadu 603 102, India

² DTN/SMTM/LMTE., bat727 p103, BP 1 C.E.Cadarache, 13108 St Paul lès Durance, France

Cabauw data, and showed the existence of z -less stratification and properties of turbulence under highly stable conditions. The hypothesis implies that dimensionless combinations of variables such as gradients, fluxes, etc. measured at the same height can be expressed as universal functions of the stability parameter (z/Λ), where Λ is the local Obukhov length. Smedman (1988) used data from the Marsta site in Sweden and showed the universality in the turbulence intensity using measurements from two different heights. Dias et al. (1995) showed that apart from second-order moments, third-order moments also followed the z -less stratification under highly stable conditions. Sorbjan (1986a, b) developed local similarity functions based on dimensional analysis and similarity approach. Each of these methods had its merits over the MOST when applied to the stably stratified boundary layer, but it failed when the surface layer became highly stable. Sorbjan (2010) further explored alternative forms of similarity scales and examined the resulting similarity laws in the stably stratified boundary layer. In contrast to the 'flux-based' MOST approach, the 'gradient-based' similarity relations worked well when the stable atmospheric layer was divided into four regimes, using the Richardson number. Overall, it is reported that the generality of any scaling law under extremely stable conditions is problematic.

Apart from atmospheric boundary layer models, another vast area of application of similarity relationships is in air pollution models. The air pollution models use the turbulence statistics of the wind components based on similarity relationships for the simulation of pollutant transport and dispersion (Hanna 1982; Kantha and Clayson 2000; Rakesh et al. 2013; Prasad et al. 2015). Functional relationships for wind velocity standard deviations, based on the MOST, are widely used in dispersion models to parameterize the diffusion. A few studies are available in the literature that addresses the behavior of normalized standard deviations of wind velocity fluctuations, especially horizontal components, under highly stable atmospheric conditions. Mahrt (1999) reported that decoupling of turbulence at higher levels with that at the surface and the motions like meandering led to the breakdown of the similarity theory, under highly stable conditions. Pahlow et al. (2001) also showed that except normalized standard deviations of temperature, normalized standard deviations of wind velocity fluctuations did not follow the similarity theory as well as the concept of z -less stratification, under highly stable conditions. Like Mahrt (1999), Baas et al. (2006), Klipp and Mahrt (2004), and Sorbjan (2006, 2010) pointed out that self-correlation played a crucial role in highly stable conditions, in predicting the success of similarity theory. This self-correlation is because the similarity theory contains shared variables on both sides of the equation leading to self-correlation. Under stable conditions, the self-correlation has the same sign as that of the expected physical correlation, leading

to an ambiguous interpretation of the results (Mahrt 2014). However, Anderson (2009) circumvented the problem of self-correlation, by fitting the relationships between individual variables, and then substituting these relationships into the ratios of interest (Mahrt 2014). Given the issues described above, we would like to examine the application of the MOST under the local scaling framework, for the stable atmospheric condition. We propose new turbulence diffusion relationships, by filtering the non-turbulent sub-mesoscale motions from the sonic anemometer data, under stable conditions for different sites, and investigate its influence on pollutant dispersion. The functional relations have new coefficients, obtained using the method of least squares regression. Before proceeding to the objective of the article, we will first briefly discuss local similarity theory based on turbulence statistics.

2 The local scaling in brief

According to the local scaling hypothesis, the dimensionless combinations of all turbulence quantities measured/computed at the same measuring heights z can be expressed as universal functions of stability parameter, $\zeta = z/\Lambda$. Pahlow et al. (2001) used a functional form which is given by

$$\frac{\sigma_i}{u_*} = A + B \left(\frac{z}{\Lambda} \right)^C \quad (1)$$

where $i = u, v, w$, and A, B , and C are empirical constants. The current study adopts the test function by Pahlow et al. (2001).

The theory and the functional relations hold good for neutral, and slightly stable regimes of the atmosphere as tested by many researchers (Dyer 1974; Hogstrom 1988).

However, investigation under the highly stable regime was not promising. The curve fit of sonic anemometer data, for normalized turbulence variables (Smedman 1988; De Bruin et al. 1993; Chu et al. 1996; Hseih and Katul 1997; Pahlow et al. 2001; Babic et al. 2016), showed that the curve of $\frac{\sigma_i}{u_*}$ is almost constant up to $\zeta = 1$. The curve turns upwards and steeply rises, for high ζ values. This upward shift in the curve indicates that the normalized turbulence quantities continue to increase and leads to more scatter under highly stable conditions. The reasons for this trend are partly due to the intermittency of turbulence that occurs during highly stable conditions (Kunkel and Walters 1981; Fernando 2003; Pardyjak et al. 2002). Additionally, the observations are sensitive to meandering (Mahrt 1998), gravity wave motions, drainage flows, and surface heterogeneity.

De Franceschi et al. (2009) reported a list of turbulence relationships proposed by various authors. In the z -less regime, when Λ is very small, the turbulence in the surface

layer is decoupled from the surface, as mentioned earlier. However, functional Eq. (1) is still valid, if locally measured scaling parameters (at the same height, where wind and temperature are measured) are used (Nieuwstadt 1984). However, when ζ becomes very large, even this local scaling seems to break down, giving way to buoyant oscillations due to gravity waves. Caughey (1977) reported such oscillations in the frequency spectrum of the wind as waves with periods varying from a few minutes to an hour. Mahrt (1998) reported that reducing the averaging time eliminates the influence of non-turbulent motions such as gravity waves, etc., particularly under very stable conditions, but the reduction in averaging time can introduce flux sampling errors. To circumvent this problem, Howell and Sun (1999) introduced the multi-resolution decomposition (MRD) of the high-frequency data, to filter out non-turbulent submesoscale motions from the sonic anemometer dataset, without compromising with errors in flux estimation.

The objective of this study is twofold. One is to establish turbulence diffusion relationships, with new coefficients, for the functional form given in Eq. (1), for the normalized standard deviations of wind velocity components, and test their applicability under stable to highly stable conditions. Fast response sonic anemometer data collected from two different sites, i.e., a hilly site Cadarache, France in the mid-latitudes, and a flat tropical coastal site Kalpakkam, India, are used for this study. The second objective is to study the dispersion of pollutants by incorporating these turbulence diffusion relationships in a Lagrangian Particle Dispersion Model, FLEXPART-WRF (Stohl et al. 2005). Further, as a case study, the gamma dose rate measured over the site Kalpakkam is used for comparison against the simulated dose rate using FLEXPART-WRF, with the new as well as the default (Hanna's) turbulence diffusion relationships.

3 Methodology

3.1 Multi-resolution decomposition

Howell and Sun (1999) proposed this method for calculating fluxes based on the relation between scale dependence of fluxes and associated flux sampling errors from time-series data. It is briefly described as follows.

If a data record has 2^l points, the data record can be divided into two sub-records, each with 2^{l-1} points. These sub-records are further divided until a sub-record contains individual datum (Howell and Sun 1999). For example, the covariance like vertical heat flux, with a cut-off scale of 2^i , starting from $(n - 1)2^i$ to $n2^i - 1$ is the average of the product of deviations, in this case, w' and θ' , from their associated means, averaged over 2^i points. The equation is given by

$$\overline{w'\theta'_n(2^i)} = \frac{1}{2^i} \sum_{j=(n-1)2^i}^{n2^i-1} [w_j - \bar{w}_n(2^i)] [\theta_j - \bar{\theta}_n(2^i)] \tag{2}$$

The associated means are as follows:

$$\bar{C}_n(2^i) = \frac{1}{2^i} \sum_{j=(n-1)2^i}^{n2^i-1} C_j \tag{3}$$

where C is any variable.

For a data record containing 2^l points, we will have 2^{l-i} sub-records for flux estimation. Each sub-record has a cut-off scale of 2^i points. For example, the vertical heat flux with a cut-off scale, 2^i over the whole data record is computed by

$$F_\theta(2^i) = \frac{1}{2^{l-i}} \sum_{n=1}^{2^{l-i}} \overline{w'\theta'_n(2^i)} \tag{4}$$

The corresponding variance over the whole set of data points is given by

$$\sigma_{F_\theta}^2(2^i) = \frac{1}{2^{l-i}} \sum_{n=1}^{2^{l-i}} [\overline{w'\theta'_n(2^i)} - F_\theta(2^i)]^2 \tag{5}$$

Assuming that 2^{l-i} values of fluxes, with a cut-off scale of 2^i over the 2^l data points are random, following Student's t distribution, then an estimate of the random flux sampling error over the data record is equal to

$$e_\theta(2^i) = \frac{t(2^{l-i}, \alpha) \sigma_{F_\theta}(2^i)}{\sqrt{2^{l-i}}} \tag{6}$$

where α is a constant parameter. This parameter is determined such that the probability that the true record averaged heat flux falling within the interval $[F_\theta - e_\theta, F_\theta + e_\theta]$ is $2\alpha - 1$ (Howell and sun 1999). Assuming a confidence level of 90%, for a large number of samples (> 30), the Student's t distribution converges to a normal distribution and the value of $t(2^{l-i}, \alpha)$ is approximately 1.3 if the confidence level is 90%, i.e., $(1-\alpha)$ from the t table.

3.2 Model configuration

For the simulation of pollutant transport and dispersion, the current study uses a Lagrangian Particle dispersion model (LPDM) FLEXPART-WRF, with Hanna's semi-empirical parameterization, relating the turbulent statistics with boundary layer scaling parameters. The FLEXPART dispersion model uses the predicted meteorological variables by the Weather Research Forecast (WRF) model for simulating the pollutant dispersion.

3.2.1 Description of the weather model, WRF

The WRF model is a mesoscale atmospheric model based on the compressible non-hydrostatic Euler equations, casted in flux form on a mass-based terrain-following vertical coordinate system. The model solves prognostic equations for the three Cartesian components of the wind velocity, various microphysical quantities, potential temperature, etc. A complete description of the WRF modeling system is available in Skamarock et al. (2005)

WRF is configured with five nested domains over the Cadarache region, with a grid size ratio of 1:3:3:3:3 (Fig. 1). The grid resolution of the master domain is 27 km, and that of the innermost domain is 0.333 km. Every domain has 100×100 grid cells.

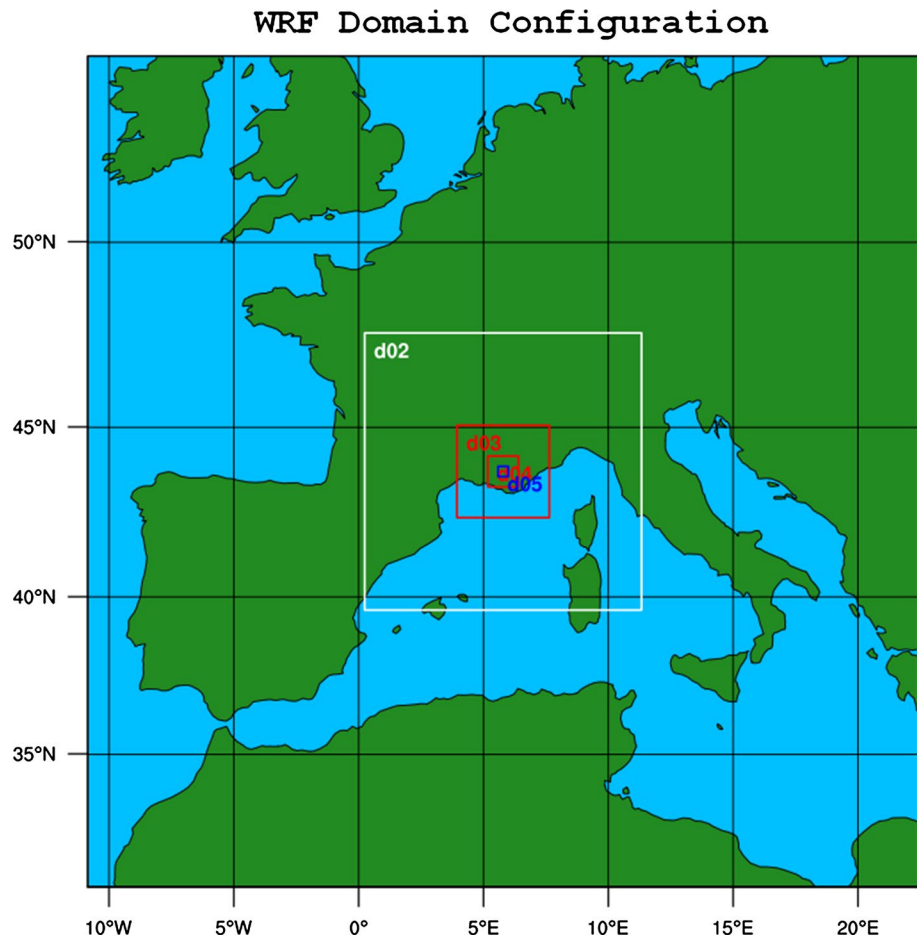
The WRF uses terrain data from United States geological survey (USGS) and land use from the moderate resolution imaging spectroradiometer (MODIS). The model employs the Mellor–Yamada–Janjic (MYJ scheme (Mellor and Yamada 1982) for boundary layer diffusion, and Janjic Eta Monin–Obukhov for surface layer scheme. The model uses the Dudhia scheme for shortwave radiation, and rapid radiative transfer model (RRTM) for longwave radiation.

WRF Single-Moment 6-Class (WSM6) microphysics and the NOAA land surface scheme are other configurations used in the model. For the cumulus option, the model uses the Grell scheme, for the 27 km domain. Each domain has 65 vertical layers, with the model top at 50 hPa. Configuration of the vertical levels is such that twenty levels are within the first 100 m, with the first model layer approximately 3 m above ground level. The model takes data from the National Centers for Environmental Prediction (NCEP) global forecast system (GFS) final (FNL) operational global analyses, for the initial and boundary conditions.

3.2.2 Brief description of FLEXPART

FLEXPART is an open-source LPDM for simulation of transport and dispersion of pollutants in the atmosphere. It is a Lagrangian particle model that uses the meteorological fields predicted by the weather prediction model WRF. The coupled FLEXPART-WRF computes particle trajectories by releasing large amounts of particles to simulate particle transport and dispersion (Stohl 2005). This model has been widely used to investigate particle transport paths and mechanisms (Wei et al. 2011; Srinivas et al. 2012; Arnold

Fig. 1 WRF simulation domain (“d” in the figure indicates the nested domain and d05 represents the innermost domain)



et al. 2015; Geng et al. 2017; Zhu et al. 2018). The theory employed is briefly described below.

The position vector of the particle at $X(t + \Delta t)$ after a time $t + \Delta t$ is given by

$$X(t + \Delta t) = X(t) + \Delta t [\bar{u}(t) + u'(t)] \quad (7)$$

where $\bar{u}(t)$ is the mean and $u'(t)$ is the fluctuating part of the wind velocity vector. The fluctuating part of the wind velocity vector, $u'(t)$ is obtained from the Langevin equation as

$$du' = -\left(\frac{u'}{\tau_L}\right)dt + \sigma_u \left(\frac{2}{\tau_L}\right)^{\frac{1}{2}} \xi(t)dt \quad (8)$$

where τ_L is the Lagrangian time scale, and $\xi(t)$ is the Gaussian random number with zero mean and unit variance. σ_u is the standard deviation of the u component of the wind. A similar relationship applies to the v component of the wind. In the case of vertical wind component, to take in to account the density stratification and well-mixed criterion, density and drift correction terms are incorporated equation. The equation used for w' in FLEXPART is as follows.

$$dw' = -w' \cdot \frac{dt}{\tau_{Lw}} + \frac{\partial \sigma_w^2}{\partial z} \cdot dt + \frac{\sigma_w^2}{\rho} \cdot \frac{\partial \rho}{\partial z} \cdot dt + \left(\frac{2}{\tau_{Lw}}\right)^{1/2} \cdot \sigma_w \cdot dW \quad (9)$$

where ρ is the air density, and dW is the incremental components of the Weiner process with mean zero and variance dt . The second and third terms in Eq. (4) are the drift correction and density corrections, respectively.

For the current study, the model generates 1,000,000 random numbers for transport and dispersion calculations for the whole simulation period. The time step of computation is small, and it is within the Lagrangian time scale for the detailed description of turbulence. By default, the model employs the Hanna' scheme (Hanna 1982) for the computation of the average standard deviation of the wind velocity vector. The WRF model supplies inputs such as wind fields, and other variables to FLEXPART every 5 min interval, to reduce the temporal interpolation errors.

4 Brief description of the observation site and measurements

Fast response sonic anemometer data over flat terrain, as well as over complex terrain, has been collected for a considerable period of a few days when the atmospheric condition is mostly stable. The study uses data from two sites with different terrain characteristics. One is a flat tropical station, Kalpakkam (12° 30' N; 80° 10' E), situated in southern

India, and the second is a hilly terrain, Cadarache (5° 44' E, 43° 42' N) in southeastern France.

4.1 Kalpakkam dataset (Case-I)

The Kalpakkam site is a coastal station, with terrain elevation varying from 6 m above mean sea level (m.s.l) at the coast to 20 m at 10 km inland. The vegetation cover comprises mainly dry, seasonally irrigated croplands and grass. The land–sea breeze circulation influences the site throughout the year. Fast response measurements use a sonic anemometer (Young make) mounted at the height of 10 m on a meteorological tower, situated about ~ 1 km away from the coast. The tower is located on a terrain with an unobstructed fetch of 300–400 m in all directions, with no buildings and obstacles around. The data-sampling rate is 10 Hz. The present analysis uses data collected for ten stable nights during November 2013. The Sonic anemometer was operational during the period 12th November–22nd November 2013, and data are archived every 30 min. The current analysis uses data collected after the sunset with positive ζ . During this period, the wind direction is predominantly northeast over this site. The site also has a 50 m meteorological tower with five levels of measurements of the meteorological parameters such as wind speed, wind direction, humidity, and temperature. Figure 2 shows the site map. The data are collected during clear sky days, free from synoptic disturbances.

4.2 Cadarache dataset (Case-II)

The Cadarache site in the Alpine foothills is topographically complex, with hills and valleys of various sizes. The area around Cadarache is heterogeneous in land use, with some agricultural fields on the Durance riverbanks, forest or bush on the hills, and a 1.3 km² lake situated northwesterly from the site. The Durance Valley (DV) is 5 to 8 km wide, with an average depth of 200 m. The portion of the DV that lies between Sisteron and the Clue de Mirabeau is 67 km in length, with a mean slope angle of 0.2° along the valley axis (Duine et al. 2017). The valley is oriented about 30° North (Fig. 3a). At the Clue de Mirabeau, the valley width varies from 5 km to 200 m. The Cadarache Valley (CV) is along the SE–NW direction. The width of the valley is 6 km long, and the width is about 1 to 2 km, with a slope angle of 1.2° along the valley.

Northeast of Cadarache is the Southern Alps, located around 70 km with a height of at least 1500 m m.s.l and up to 3000 m at a distance of 140 km. Two east–west orientated mountain ridges viz-a-viz the Luberon and the Sainte Victoire are at a moderate distance from the site. Both have maximum heights of 1000–1100 m. The measurement location is a flat area with bushes in the south, and a few distant



Fig. 2 The site map of Kalpakkam. The red circle shows the location of the meteorological tower and sonic anemometer. The balloon with a star shows the locations of environmental radiation monitors (Courtesy: Google Maps)

low buildings (1 or 2 storeys) in the north and northwest sector. The fetch is 400 m along the small Cadarache valley axis and about 200 m crosswise the valley. The measuring mast is installed right in the middle of this open prairie. The nearest buildings are 120 m away from the measurement location. The winds from north and northwest, like Mistral or summer sea breeze, are generally associated with neutral to unstable conditions. Therefore, the analysis does not include the data recorded during the north and northwesterly winds. We make use of an intensive observation period (IOP) dataset collected during the KASCADE experiment (KAtabatic winds and Stability over Cadarache for the Dispersion of Effluents) (Duine et al. 2017). Concerning the purpose of the field measurement campaign, the most favorable weather

conditions occur when clear skies are present, and when the influence of synoptic systems on the local wind field is weak. As it is very likely to have these conditions during the winter months in the region, it was decided to follow a negative warning concept, i.e., when low-pressure systems are in the vicinity or Mistral will occur; the planned IOP's will not be conducted. The current study uses the data from sonic anemometer (Young make) collected at 10 m above ground level, for a few stable nights, with clear sky in February 2013 (10th February to 20th February), free from synoptic disturbance. The sampling rate is 10 Hz. The site also has a sonic anemometer mounted at a height of 2 m above ground level. The stable boundary layer (SBL) height varies between 13 and 27 m during this period. The SBL height is estimated

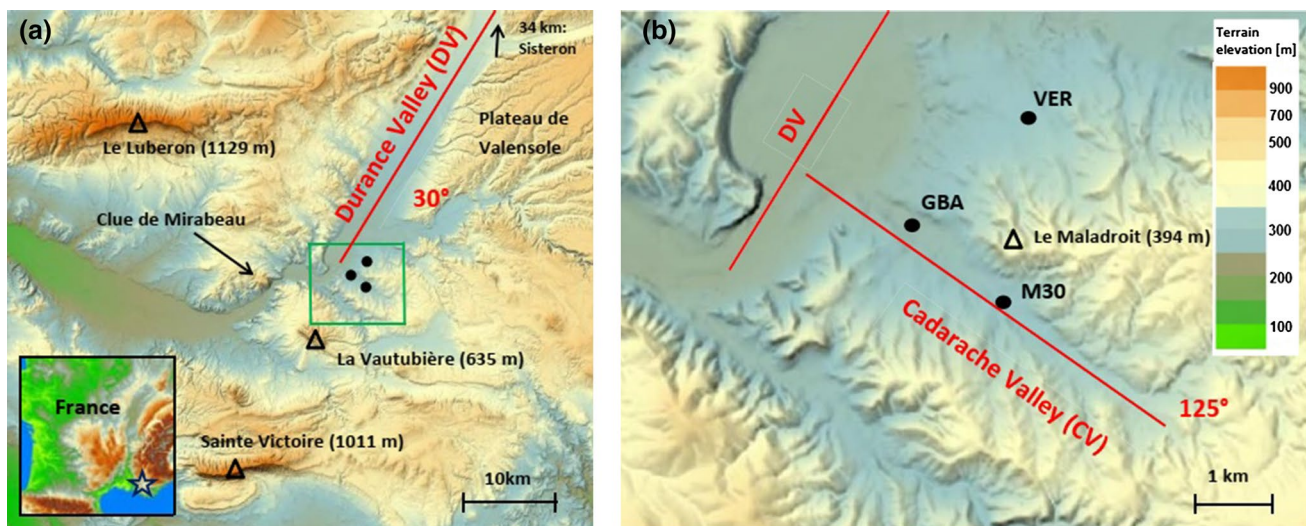


Fig. 3 **a** provides study area in lower left frame, **b** is the enlargement of the green rectangle in **(a)**. The red lines show the Durance (DV) and the Cadarache (CV) valleys, respectively. Black dots indicate the

using the formulations listed in Zilitinkevich and Baklanov (2002). The location of the sonic anemometer is shown as M30 in Fig. 3b. The data cover a wide range of stable atmospheric conditions, including highly stable conditions with a ζ value of 10. The raw data are archived every 30 min. Each night contains varying hours of stable conditions. Further, tether sonde (TS) observations available during the period February 17th to February 19th, 2013 were used for vertical profile comparison of simulated wind speed and wind direction, using WRF. The location of the TS is marked as VER in Fig. 3b. The maximum height of TS achieved was 250 m above ground level during this period.

5 Data analysis

The data used for the analysis are quality checked. The data are visually inspected to check the presence of spikes by plotting the time-series data. Then, the data are de-trended, and the coordinate system is rotated relative to the streamline direction, using double rotation and tilt correction. Under the highly stable condition, to avoid the inadvertent capture of non-turbulent motions in the calculation of standard deviation of wind velocity components (Smedman 1988; Mahrt et al. 1998; Mahrt 1999), the averaging time is chosen based on the MRD method. The analysis considers only data points that comply with the Taylor hypothesis. Many researchers (Stull 1988; Pahlow et al. 2001) suggested that the Taylor hypothesis is valid when the turbulence intensity is smaller than the mean

measurement locations. Courtesy: The Royal Meteorological Society (Duine et al., 2017, Quarterly Journal of Royal Meteorological Society)

wind speed. This condition is satisfied by computing the turbulence intensity, $\frac{\sigma_u}{U}$, and applying the criterion that the data with $\frac{\sigma_u}{U} > 0.5$ is rejected (Pahlow et al. 2001). The data points after the rejection are reduced to 473 from 532 for the Cadarache dataset and 348 from 403 for the Kalpakkam dataset.

Given below are the various scaling parameters required for the computation of turbulence intensity in the framework of the local similarity theory.

The local Obukhov length is given by

$$\Lambda = \frac{-\tau^{\frac{3}{2}} T'}{g\kappa w' T'} \quad (10)$$

The expression for the shear stress is given by

$$\tau = \rho \left[(\overline{uw})^2 + (\overline{vw})^2 \right] \quad (11)$$

where ρ is the air density.

The prime quantities refer to the turbulence fluctuations about the mean. κ is the Von Karman constant accepted as 0.4.

The normalized wind velocity standard deviations $\left(\frac{\sigma_i}{u_*}\right)$, where i being u, v, w , and the stability parameter $\left(\frac{z}{\Lambda}\right)$ (where z is the measurement height), are computed using the scaling variables u_* and Λ . Equation (1) shows the profile relation for normalized components of wind velocity standard deviations, for the stable condition based on the local similarity theory. The study uses the method of least square regression for fitting values of $\left(\frac{\sigma_i}{u_*}\right)$ against $\left(\frac{z}{\Lambda}\right)$.

6 Results

6.1 Results of multi-resolution decomposition

6.1.1 Multi-resolution decomposition on Kalpakkam datasets

This analysis uses sonic anemometer data from ten stable nights. Figure 4 shows the MRD spectrum following the algorithm, suggested by Howell and Sun (1999) for heat and momentum flux. Here, ΔF is the change in flux of heat or momentum between adjacent cut-off scales, F is the flux of heat or momentum, and Δe is the flux error. The flux error, Δe is calculated by assuming that the heat flux, with different cut-off scale, follows Student's t distribution (Howell and Sun 1999).

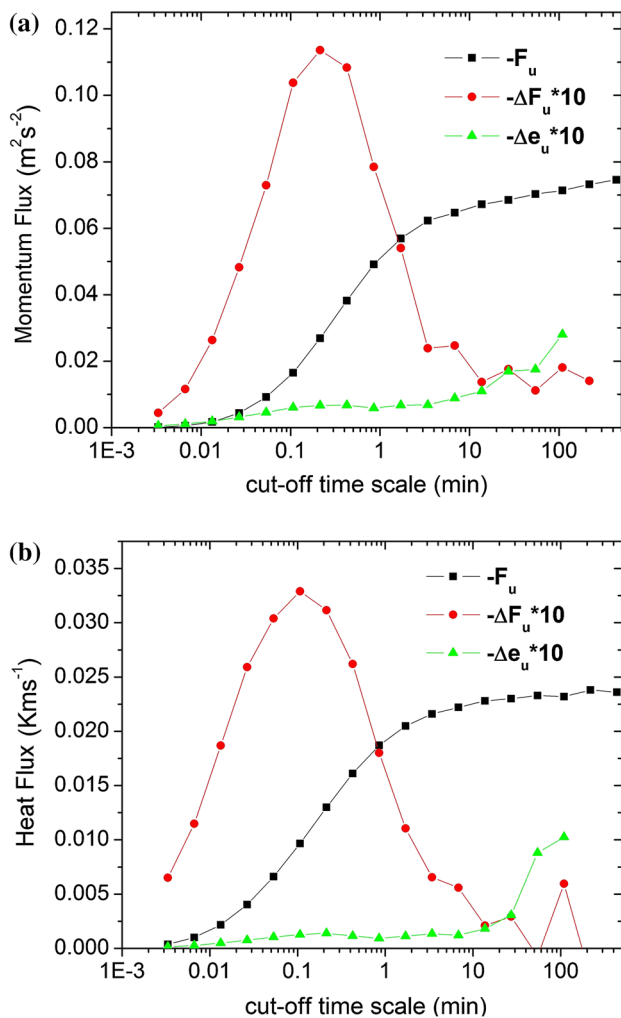
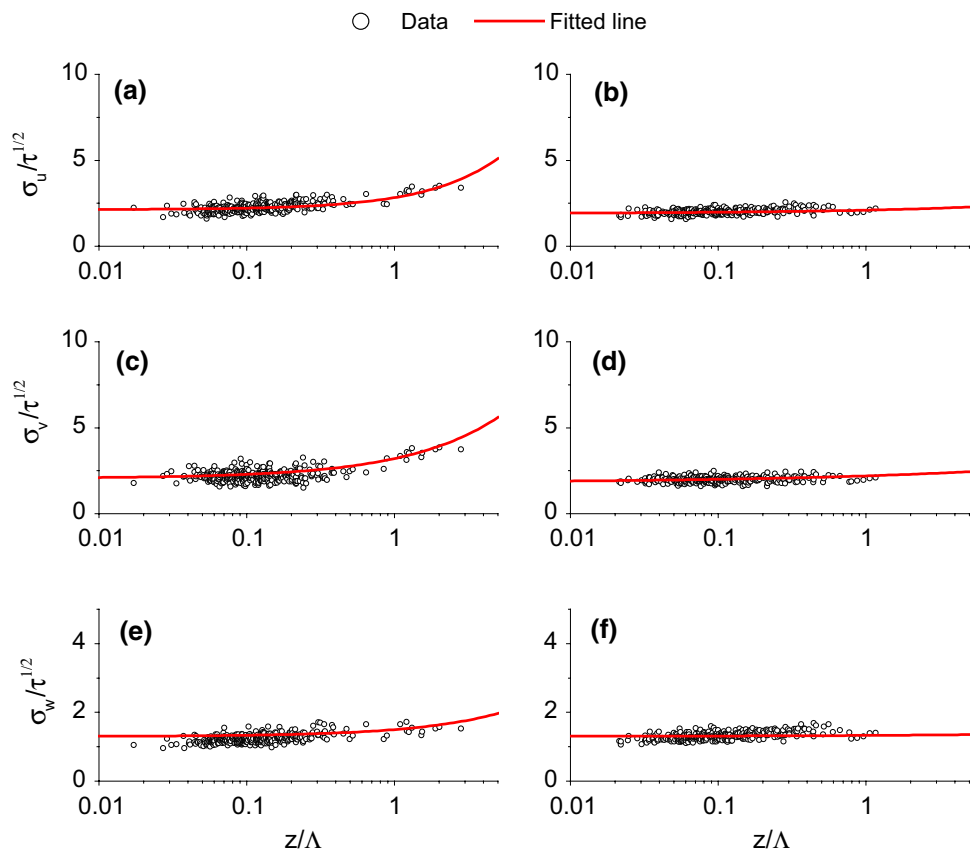


Fig. 4 a The multi-resolution decomposition plot for momentum. b The multi-resolution decomposition plot for Heat

Figure 4a as well as Fig. 4b indicates that above the cut-off scale of ~ 15 min, the flux sampling error (Δe) is more than the change in fluxes (ΔF) between successive cut-off scales. In this case, it implies that choosing a time record length, spanning more than 15 min, will introduce errors in the flux estimates. Using this result as guidance, and taking in to account of variations in the cut-off scale for different sub-record, we choose 15 min as the time scale for each sub-record, for the estimation of fluxes. The cut-off scale is the record length of the data, that can be used for flux estimate with confidence, without any flux sampling errors. Further, the fluxes for each sub-record are estimated by finding out the cut-off scale within each sub-record and averaging the fluxes for these sub-records. The cut-off scale, within each sub-record, is estimated at the point where $\Delta e < \Delta F$ in the flux-error curve, similar to Fig. 4. Different sub-records show different cut-off scales. The minimum cut-off scale was found to be ~ 1 min for flux computation. The fluxes thus estimated are used for the computation of the local Obukhov length, Λ and subsequently for estimation of shear stress. The shear stress and the Obukhov length are further used for estimating scaled standard deviations as a function of ζ . Figure 5 shows the normalized standard deviation of horizontal and vertical components of the wind velocity, calculated with and without MRD.

The figure indicates that the scatter in the data of normalized turbulence components for stable conditions is less with the MRD over the one without MRD. Basu et al. (2006) also obtained similar results. The figure also indicates that relationships without filtering show an increasing trend for $\zeta \approx 0.5$. Pahlow et al. (2001) and Mahrt et al. (1998) reported the constancy in the value of the horizontal wind component up to $\zeta \leq 0.1$. Smedman (1988) and Babic et al. (2016) reported the constancy up to $\zeta \leq 0.5$. Similarly, De Franceschi et al. (2009) reported the constancy up to $\zeta \approx 1$ after applying the appropriate filter. Many researchers (Smedman 1988; De Bruin et al. 1993; Chu et al. 1996; Hsieh and Katul 1997; Pahlow et al. 2001) reported the increase in the value of $\frac{\sigma_z}{u_*}$, for high ζ . A few studies in the tropical and coastal areas (Dharamaraj et al. 2009; Prasad et al. 2015, 2018) also show an increase in the value of normalized turbulence quantities, under stable conditions. However, this increase in the value of $\frac{\sigma_z}{u_*}$ is not conspicuous, after filtering out the non-turbulent motions from the dataset, in this case by MRD. The figure indicates that the rise in the value of normalized turbulence quantities, with the MRD, is lesser at the highly stable regime, compared to that estimated without MRD. Further, the figure shows that the number of data points is meager in near-neutral and neutral conditions. The less number of data at near-neutral conditions is because, at Kalpakkam, the number occurrences of near-neutral and neutral stability conditions are not frequent.

Fig. 5 The Normalized standard deviation of horizontal and vertical wind components without (left panel) and with (right panel) multi-resolution decomposition



Extrapolation of the fitted curve (Fig. 5b, d, f) of normalized standard deviation against ζ , to neutral conditions, shows a value of 1.8 ± 0.03 , 1.9 ± 0.06 , and 1.1 ± 0.04 for the empirical constant A, for normalized horizontal (u and v components) and vertical standard deviations, respectively, with 95% confidence level. Pahlow et al. (2001) reported the value of the constant A as 2.3, 2, and 1.1, respectively, for u , v , and w component of the normalized wind velocity standard deviations. Similarly, Smedman (1988) reported the value of A as 2.3, 1.7, respectively, for u and v velocity standard deviations. Further, Panofsky and Dutton (1984) reported this value as 2.4 and 1.9, respectively, for u and v velocity standard deviations. De Franceschi et al. (2009) reported this value for along-valley wind as 1.92 ± 0.02 and 1.71 ± 0.02 , for u component and v component of the standard deviations and 1.32 ± 0.01 , for w component of the standard deviation. Similarly, for cross valley winds, they reported these values to be 1.90 ± 0.09 , 1.89 ± 0.08 and 1.38 ± 0.05 , for u , v , and w component of the standard deviations. Babic et al. (2016) reported these values for different heights over industrial town Kutina in Croatia, under wintertime nocturnal conditions.

Our estimates of the constant B for horizontal and vertical components of turbulence are 0.4, 0.2, and 0.4, respectively, with a 95% confidence level. The value of C is 0.3, for all

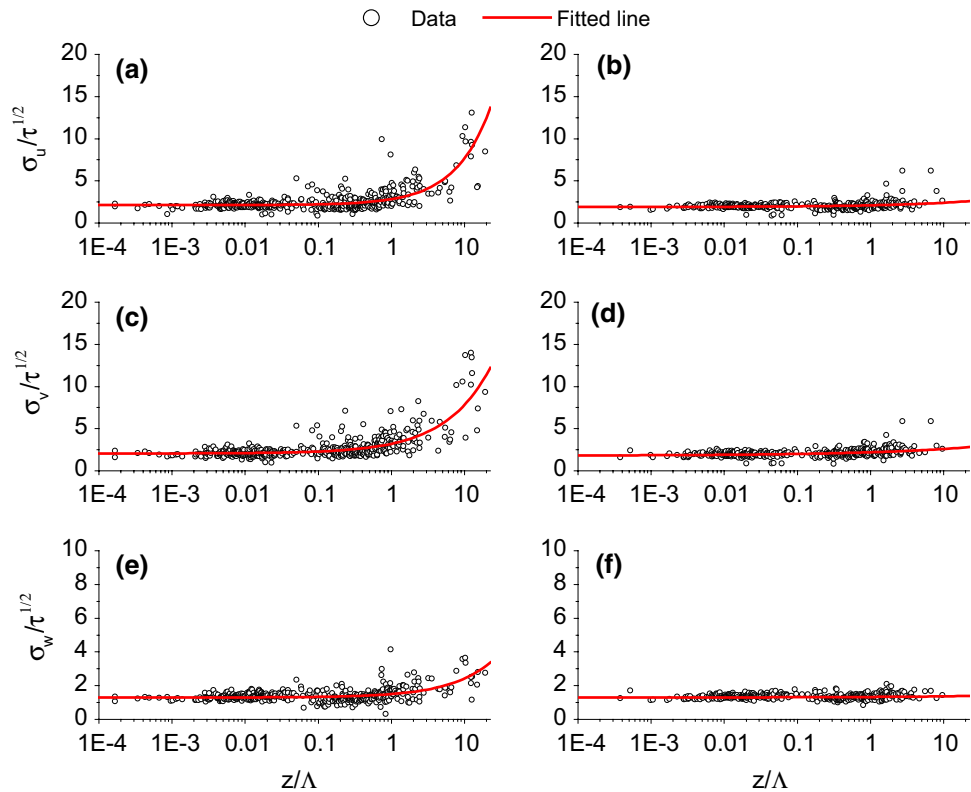
the components. The increase in the value of normalized turbulence, for high ζ is not observed in this case, due to the filtering of non-turbulent motions. The constancy of the values of $\frac{\sigma_i}{u_*}$, at the stable regime indicates that the relationships derived for the Kalpakkam site, follow local similarity theory, under stable atmospheric conditions. The next section discusses the results of a similar analysis carried out for the Cadarache data.

6.1.2 Multi-resolution decomposition of Cadarache dataset

Similar multi-resolution decomposition to the Cadarache data shows the cut-off time scale as 10 min instead of 15 min as the case of the Kalpakkam site (Figure not shown). Analysis of different data records for the Cadarache region shows a minimum cut-off scale of ~ 1 min, similar to Kalpakkam. Figure 6 shows the normalized standard deviations, with and without multi-resolution decomposition.

The Fig. 6 indicates that without MRD, more scatter is observed in the value of the normalized components, and shows an upward trend in the curve for $\zeta > 1$ (Fig. 6a, c, e). The rise in the curve (left panel), for higher values of ζ , shows the influence of the non-turbulent motions, on the normalized standard deviations of wind velocity.

Fig. 6 The Normalized standard deviation of horizontal and vertical wind without (left panel) and with (right panel) multi-resolution decomposition



The figure also conveys that the slope of the curve in the left panel is higher than the slope noticed in the case of Kalpakkam data. On the other hand, the values of normalized standard deviations did not show such scatter and upward trend after filtering of the non-turbulent motions. The extrapolation of the fitted curve of values of normalized standard deviations (Fig. 4b, d, f) to neutral conditions shows a value of 1.9 ± 0.07 , 1.8 ± 0.06 , and 1.3 ± 0.02 for the constant A for horizontal and vertical components, respectively, with 95% confidence level, which is closer (less than 10%) to the values obtained for the Kalpakkam dataset, except for the vertical component (less than 20%). Many researchers (Nieuwstadt 1984; Smedman 1988; De Bruin et al. 1993; Chu et al. 1996; Mahrt et al. 1998; Pahlow et al. 2001; Babic et al. 2016) analyzed the w component of wind velocity standard deviation. In a review of turbulence statistics, Dias and Brutsaert (1996) reported the value of A from several works and mentioned that it centers around 1.3. Similarly, for the constant B, the curve fit shows a value of 0.2, 0.3, and 0.03, respectively, for horizontal and vertical turbulence intensities, with a 95% confidence level. The value of C is 0.4 for longitudinal and vertical components, and 0.3 for crosswind components. Table 1 summarizes the empirical formulation for normalized wind velocity standard deviations obtained from both sites.

Table 1 Normalized corrected wind velocity standard deviations under stable conditions

Site	U direction	V direction	W direction
Cadarache	$1.9 + 0.2\left(\frac{z}{L}\right)^{0.4}$	$1.8 + 0.3\left(\frac{z}{L}\right)^{0.3}$	$1.3 + 0.03\left(\frac{z}{L}\right)^{0.4}$
Kalpakkam	$1.8 + 0.4\left(\frac{z}{L}\right)^{0.3}$	$1.9 + 0.2\left(\frac{z}{L}\right)^{0.3}$	$1.1 + 0.4\left(\frac{z}{L}\right)^{0.3}$

6.2 Simulation of dispersion using FLEXPART-WRF

6.2.1 Results of FLEXPART-WRF simulation over Cadarache

The new turbulence diffusion formulations obtained for the Cadarache site are incorporated in the FLEXPART model, to study the effect of new functional relationships on dispersion. As already mentioned, the WRF provides inputs for the FLEXPART model. The WRF is initialized at 1200 GMT on 17th February 2013, during one of the IOP and integration is continued until 1200 GMT on 19th February 2013. The FLEXPART simulation assumes a ground-level release with a release rate of 1 g/s. The main inputs to FLEXPART are three components of the wind velocity and the surface layer scaling parameters (u^* , L , mixed layer height). The wind speed and direction simulated by the WRF are compared with observations at 10 m above ground level, starting from

1200 GMT 17th February 2013 for 48 h and is shown in Fig. 7.

The root mean square error (RMSE) for wind speed is 1.35 m/s, and for the wind direction, it is 61.5°. The high value of RMSE is also reported by others as well (Seaman et al. 2012), especially under low wind speed. Moreover, at very low wind speeds, the observed wind directions are not very reliable (Soler et al. 2011). Further, Fig. 8a–d shows the comparison plot of the simulated vertical profiles of wind speed and wind direction with tethersonde observation, available during the IOP at 1600 GMT on 18th February 2013, 2000 GMT on 18th February 2013, 0800 GMT on 19th February 2013 and 2000 GMT on 19th February 2013, respectively.

The simulated vertical profiles at both the times are in good agreement with observation. The estimated RMSE for wind direction and wind speed are 21.71°, 1.35 m/s, 13.77°, 0.47 m/s, 42.64°, 1.02 m/s, and 23.82°, 1.25 for Fig. 8a–d, respectively. Further, for dispersion simulation, the FLEXPART model is initialized at 1800 GMT on 18th February 2013 and integrated till 1200 GMT on 19th February 2013 so that the simulation covers the stable atmospheric conditions. The study further compares the gamma dose rate simulated by FLEXPART, using the new relationships (Table 1) and the model default Hanna’s method (Hanna 1982). The model uses the point kernel method (Oza et al. 1999; Rakesh et al. 2015; Srinivas et al. 2017), for gamma dose rate computation. The similarity relationships for normalized wind velocity standard deviations formulated by Hanna, for stable conditions are recalled below.

$$\sigma_u = 2u_* \left(1 - \frac{z}{h}\right) \tag{13}$$

$$\sigma_v = 1.3u_* \left(1 - \frac{z}{h}\right) \tag{14}$$

$$\sigma_w = \sigma_v \tag{15}$$

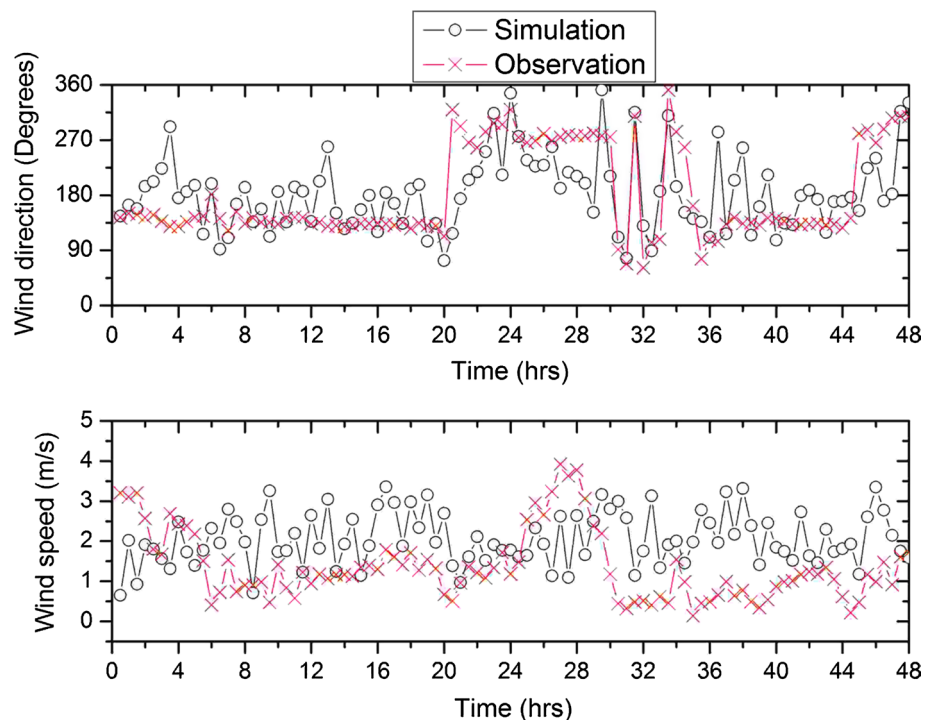
Here, h is the boundary layer height.

Figure 9 shows the color-shaded maps of relative dose patterns during 2 night hours (0023 GMT and 0000 GMT) under highly stable atmospheric conditions.

The analysis time corresponds to an atmospheric condition with positive values of ζ . The left panel shows the dose rate with the new scheme relative to the default Hanna’s scheme at 0023 GMT, and the right panel shows the same, but at 0000 GMT. From the figure, it is evident that the new scheme simulates a higher dose rate relative to the model default scheme. Spatially, the dose rate, with the new scheme, shows a variation between a factor of 1.2–2 relative to Hanna’s scheme. Moreover, the figure also shows that the relative dose rate is lower, 0.2–0.5, especially at the lateral boundary of the plume, i.e., the dose rate simulated using Hanna’s scheme is higher than the dose rate simulated with the new method. This lower relative dose is because Hanna’s scheme simulates higher diffusive velocity, and thereby more dispersion and broader plume.

On the other hand, the new scheme simulates less dispersion and narrower plume, thereby leading to a lower relative dose rate at the boundary of the plume. Seaman

Fig. 7 Comparison of simulated wind speed and wind direction at 10 m with observation



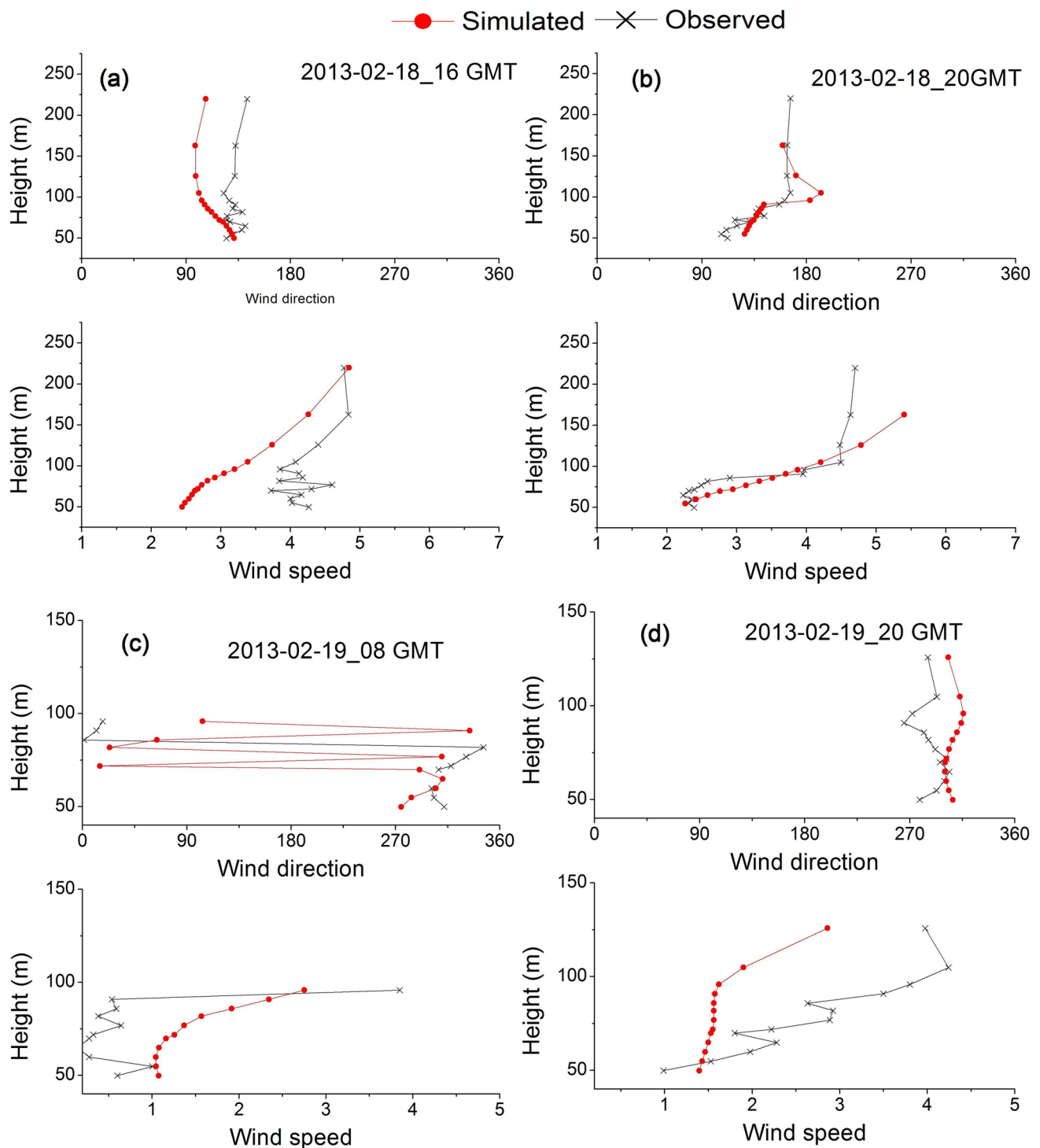
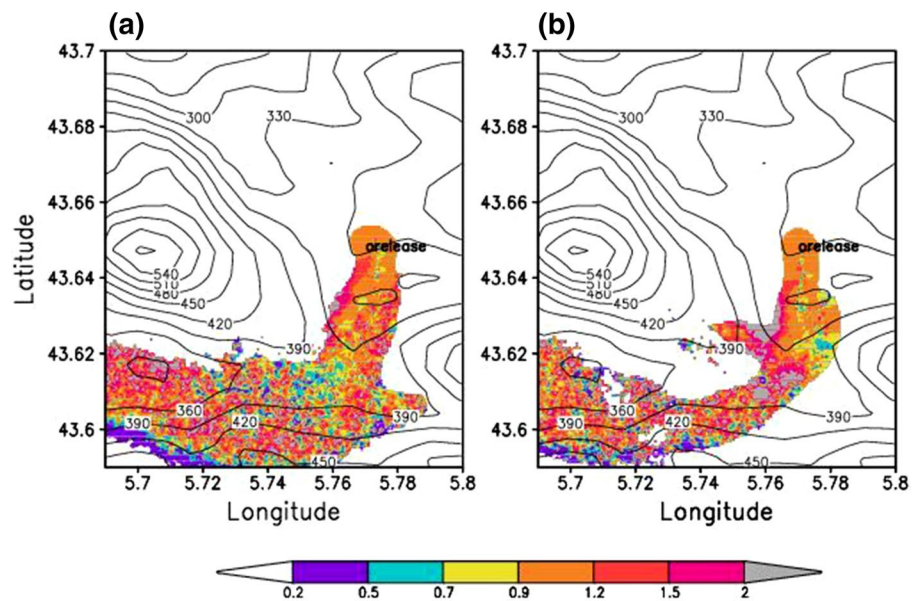


Fig. 8 Comparison of the vertical profile of wind speed and wind direction at **a** 1600 GMT on 18th February 2013, **b** 2000 GMT on 18th February 2013, **c** 0800 GMT on 19th February 2013 (**d**) and 2000 GMT on 19th February 2013

et al. (2012) reported that high-resolution simulation using weather models like WRF could simulate submesoscale motions, only to some extent. However, in dispersion calculations, it is required to use the turbulent diffusion

relationships free from such motions, for a conservative estimate of dispersion, especially while using high-resolution weather models like WRF. Otherwise, it leads to the accounting of such motions twice in dispersion estimates,

Fig. 9 The relative (to Hanna's method) gamma dose rate simulated using new turbulence diffusion method at 0023 GMT and 0000 GMT. The contour refers to the topographic height



thereby underestimating the pollutant concentration. This is especially crucial in the case of radioactivity dispersion since the regulatory limits for nuclear power plant releases are fixed based on the simulated dose calculations using these types of dispersion models coupled with weather models.

For the validation of the above dispersion calculations, no experimental tracer concentration data are available at this site, Cadarache. However, at Kalpakkam, the plume gamma dose rate is monitored using a network of environmental radiation monitors (ERM) around the Madras Atomic Power Station (MAPS). The plant (MAPS) releases trace quantities of radioactive Argon gas under normal operating conditions, from a 100 m stack. The dose rate data collected using ERMs used further for comparison with the simulated plume dose rate, and the next section discusses these results.

6.2.2 Comparison of FLEXPART simulation with observations over Kalpakkam

The site Kalpakkam has ERMs mounted at 1 m above ground level in each wind direction sector of 22.5° width. The detectors are arranged in a two-ring fashion, one ring at 500 m away from the release point (MAPS), and the other ring at 1500 m. There are a total of 27 monitors around the release point. Figure 2 shows the pictorial representation of sampler locations. The ERMs record the gamma dose rate (nGy/h) due to normal operational releases from the reactor, using Geiger Muller counters. The details of the releases and the ERM network are available in Srinivas et al. (2017). The ERMs record the gamma dose due to normal releases from the power plant. The background radiation dose at a particular detector location is estimated when the radiation

plume is not over that particular detector. The recorded dose rate by the detector is the total dose rate due to the natural background and the argon releases from the reactor. The actual dose due to releases from the power plant is obtained by subtracting the background at ERM location, from the total dose rate registered in the ERM. The current study uses the gamma dose rate data collected during November 2016, and during this period, the wind direction is predominantly northeast, and the impact of the radioactive plume is over the land. Further, during the nighttime, the atmospheric stability ranges from Pasquill class "E" to "F" over this region. The present analysis uses 65 h of data of gamma dose rate collected under stable atmospheric conditions. For the simulation of dose rates and further comparison with measured dose rates, the FLEXPART model uses input data from the meteorological tower for dispersion estimates. When the argon plume passes over the detector, the detector shows a spike in the time-series data of the dose rate. As the wind is from the northeast, the detectors in the southwest sector relative to the reactor show the increase in dose rate. Two detectors of the network captured the radioactive plume for the flow direction during these hours as the rest of them were away from the primary impacted sector. Figure 10 shows the correlation plot of the observed gamma dose rate against simulated values, with the new and Hanns's method of computing wind velocity standard deviations. Both the observed as well as simulated dose rate values are normalized with the observed maximum dose rate.

The figure indicates that the incorporation of the new relationships for turbulent intensities for stable atmospheric conditions in FLEXPART produces better results for the dose rate estimates compared to the model default Hanna's method. Table 2 shows the error statistics.

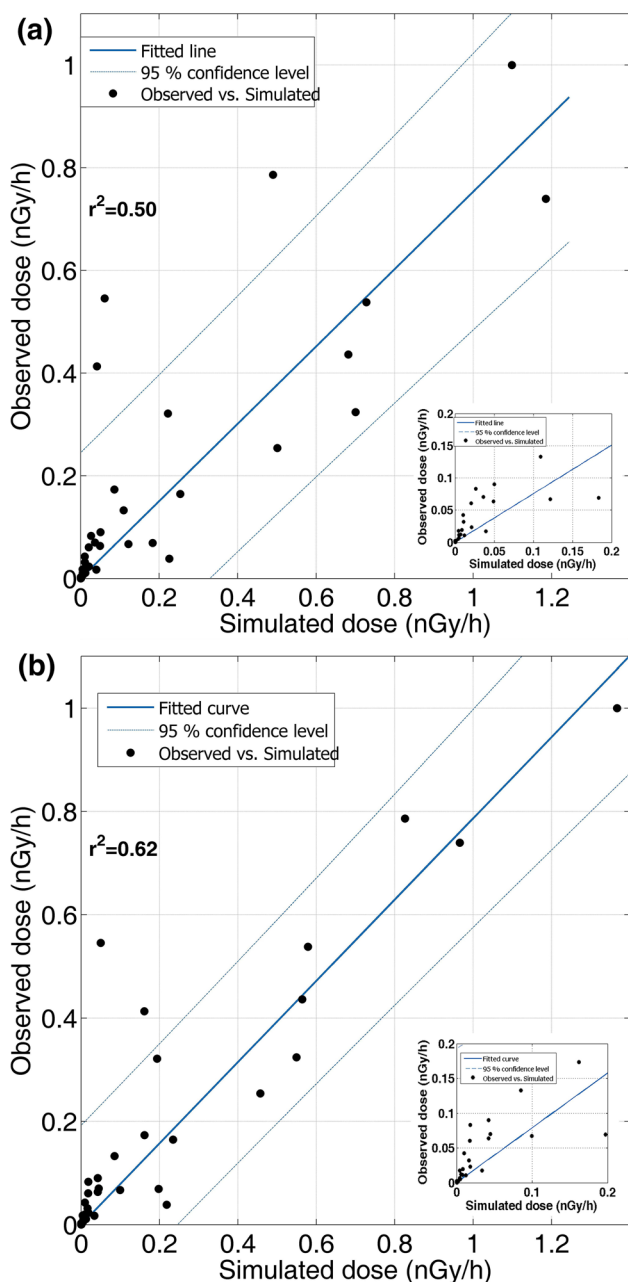


Fig. 10 Comparison of observed and simulated gamma dose using **a** Hanna's method, **b** new method for turbulence diffusivity. The inset shows the zoomed image between 0 and 0.2 nGy/h

Table 2 indicates that the new schemes perform better compared to the default scheme. Though the turbulence coefficients in the corresponding relationships are different, the difference is not very evident in the dose estimates because of less number of data in the highly stable regime over Kalpakkam. It is challenging to get the coincidence of highly stable conditions and the radioactive plume centerline over the detectors. For better statistics, it is necessary to analyze dose records under more events

Table 2 The dose rate error statistics with Hanna's method and the new method

Error	Hanna's scheme	New scheme
FB	-0.06	-0.06
NSME	1.18	0.77
MG	1.70	1.60
VG	3.40	3.10
FAC2	0.37	0.51
R2	0.50	0.62

of stable conditions. Nevertheless, the present study indicates an improvement in dispersion estimates under highly stable atmospheric conditions.

7 Conclusions

The present study shows that under stable conditions, the normalized standard deviation of the wind components follows local similarity theory if non-turbulent motions are filtered. The study also indicates that the values of the empirical coefficients vary within 10%, in the case of horizontal wind and ~20% in the case of vertical wind velocity standard deviations, for the flat terrain of Kalpakkam and the hilly complex Cadarache terrain, considered for the study. The study used multi-resolution decomposition to filter the non-turbulent motions from the fast response measurements. The simulation with new turbulence diffusion relationships in the FLEXPART model indicates that the simulated gamma dose rates are improved compared to the model default Hanna's method. The results also show that new turbulence relationships predict narrower plume and higher dose rate compared to the Hanna's scheme under stable atmospheric conditions. The study used measured dose rate data from two detectors since they matched the requirement of the meteorological condition though it is inadequate for arriving at a statistically robust conclusion. Nevertheless, the study indicates that the new relationships show promising results in simulating the dispersion under highly stable conditions. The study is essential, especially in the context of radioactivity dispersion, since it warrants conservative estimates of radiological dose.

Acknowledgements Authors express their sincere thanks to Director, Indira Gandhi Center for Atomic Research. Station Director, Madras Atomic Power Station, is acknowledged for providing the Ar⁴¹ release data used in the present study. Authors convey special thanks to the KASCADE team (Commissariat à l'énergie atomique et aux énergies alternatives-DEN-Cad/Laboratoire de Modélisation des Transferts dans l'Environnement and Laboratoire d'Aérodynamique UMR 5560) for providing the datasets for the present study. The KASCADE dataset is now available at <https://kascade.sedoo.fr>.

References

- Anderson P (2009) Measurement of Prandtl number as a function of Richardson number avoiding self correlation. *Bound Layer Meteorol* 131:345–362
- Arnold D, Maurer C, Wotawa G, Draxler R, Saito K, Seibert P (2015) Influence of the meteorological input on the atmospheric transport modelling with FLEXPART of radionuclides from the Fukushima Daiichi nuclear accident. *J Environ Radioact* 139:212–225
- Baas P, Steeneveld G, van de Weil B, Holtslag A (2006) Exploring self-correlation in the flux-gradient relationships for stably stratified conditions. *J Atmos Sci* 63:3045–3054
- Babić K, Rotach MW, Klaić ZB (2016) Evaluation of local similarity theory in the wintertime nocturnal boundary layer over heterogeneous surface. *Agric For Meteorol* 228:164–179
- Basu S, Porte-Agel F, Foufoula-Georgiou E, Vinuesa JF, Pahlow M (2006) Revisiting the local scaling hypothesis in stably stratified atmospheric boundary-layer turbulence: an integration of field and laboratory measurements with large-eddy simulations. *Bound Layer Meteorol* 119:473–500
- Belušić D, Mahrt L (2008) Estimation of length scales from mesoscale networks. *Tellus A: Dyn Meteorol Oceanogr* 60(4):706–715
- Businger J, Arya SPS (1974) Height of the mixed layer in the stably stratified planetary boundary layer, advances in geophysics, 18A. Academic Press, New York, pp 73–92
- Businger JA, Wyngaard JC, Izumi Y, Bradley EF (1971) Flux-profile relationships in the atmospheric surface layer. *J Atmos Sci* 28(2):181–189
- Caughy SJ (1977) Boundary-layer turbulence spectra in stable conditions. *Bound Layer Meteorol* 11(1):3–14
- Chu CR, Parlange MB, Katul GG, Albertson JD (1996) Probability density functions of turbulent velocity and temperature in the atmospheric surface layer. *Water Resour Res* 32:1681–1688
- De Bruin HAR, Kohsiek W, van den Hurk JJM (1993) a verification of some methods to determine the fluxes of momentum, sensible heat, and water vapour using standard deviation and structure parameter of scalar meteorological quantities. *Bound Layer Meteorol* 63:231–257
- De Franceschi M, Zardi D, Tagliuzucca M, Tampieri F (2009) Analysis of second-order moments in surface layer turbulence in an Alpine valley. *Q J R Meteorol Soc* 135(644):1750–1765
- Dharamaraj T, Chintalu GR, Raj PE (2009) Turbulence characteristics in the atmospheric surface layer during summer monsoon of 1997 over a semi-arid location in India. *Meteorol Atmos Phys* 104:113–123
- Dias NL, Brutsaert W (1996) Similarity of scalars under stable stratification. *Bound Layer Meteorol* 80:355–373
- Dias NL, Brutsaert W, Wesley ML (1995) z-Less stratification under stable conditions. *Bound Layer Meteorol* 75:175–187
- Duine GJ, Hedde T, Roubin P, Durand P, Lothon M, Lohou F, Augustin P, Fourmentin M (2017) Characterization of valley flows within two confluent valleys under stable conditions: observations from the KASCADE field experiment. *Q J R Meteorol Soc* 143(705):1886–1902
- Dyer AJ (1974) A review of flux-profile relationships. *Bound Layer Meteorol* 7(3):363–372
- Emeis S (2010) A simple analytical wind park model considering atmospheric stability. *Wind Energy* 13(5):459–469
- Emeis S (2013) Wind energy meteorology—atmospheric physics for wind power generation. Springer, Dordrecht, p 150
- Fernando HJS (2003) Turbulent patches in a stratified shear flow. *Phys Fluids* 15(10):3164
- Garratt JR (1994) The atmospheric boundary layer. *Earth Sci Rev* 37(1–2):89–134
- Geng X, Xie Z, Zhang L (2017) Influence of emission rate on atmospheric dispersion modeling of the Fukushima Daiichi nuclear power plant accident. *Atmospheric Pollution Research* 8(3):439–445
- Hanna SR (1982) Applications in air pollution modeling. In: Nieuwstadt FTM, van Dop H (eds) *Atmospheric turbulence and air pollution modelling*. Reidel, Boston
- Högström U (1988) Non-dimensional wind and temperature profiles in the atmospheric surface layer. a re-evaluation. *Bound Layer Meteorol* 42:55–78
- Howell JF, Sun J (1999) Surface-layer fluxes in stable conditions. *Bound Layer Meteorol* 90:495–520
- Hsieh CI, Katul GG (1997) Dissipation methods, Taylor's hypothesis, and stability correction functions in the atmospheric surface layer. *J Geophys Res* 102:16391–16405
- Kantha LH, Clayson CA (2000) *Small scale processes in geophysical fluid flows*. Academic Press, San Diego, p 883
- Klipp C, Mahrt L (2004) Flux-gradient relationship, self-correlation and intermittency in the stable boundary layer. *Q J R Meteorol Soc* 130:2087–2104
- Kunkel KE, Walters DL (1981) Intermittent turbulence in measurements of the temperature structure parameter under very stable conditions. *Bound Layer Meteorol* 22:49–60
- Lange M, Focken U (2005) *Physical approach to short-term wind power prediction*. Springer, Berlin, p 167
- Mahrt L (1998) Stratified atmospheric boundary layers and breakdown of models. *Theor Comput Fluid Dyn* 11:263–279
- Mahrt L (1999) Stratified atmospheric boundary layers. *Bound Layer Meteorol* 90:375–396
- Mahrt L (2011) Surface wind direction variability. *J Appl Meteorol Clim* 50(144–152):2011. <https://doi.org/10.1175/2010JAMC2560.1>
- Mahrt L (2014) Stably stratified atmospheric boundary layers. *Annu Rev Fluid Mech* 46:23–45
- Mahrt L, Vickers D (2006) Extremely weak mixing in stable conditions. *Boundary-Layer Meteorol* 119(1):19–39
- Mellor GL, Yamada T (1982) Development of a turbulence closure model for geophysical fluid problems. *Rev Geophys* 20(4):851–875
- Mestayer PG, Anquetin S (1995) Climatology of cities. In: Gyr A, Rys F-S (eds) *Diffusion and transport of pollutants*. Kluwer Academic, New York, pp 165–189
- Monin AS, Obukhov AM (1954) Basic laws of turbulent mixing in the ground layer of the atmosphere. *Trans Geophys Inst Akad Nauk USSR* 151:163–187
- Monteiro C, Bessa R, Miranda V, Botterud A, Wang J, Conzelmann G (2009) *Wind power forecasting: state of-the-art 2009*. Argonne National Laboratory, Lemont, p 216
- Nieuwstadt FTM (1984) The turbulent structure of the stable, nocturnal boundary layer. *J Atmos Sci* 41:2202–2216
- Oza RB, Daou VJ, Sitaraman V, Krishnamoorthy TM (1999) Plume gamma dose evaluation under non-homogeneous non-stationary meteorological conditions using particle trajectory model for short term releases. *Radiat Prot Dosim* 82(3):201–206
- Pahlow M, Parlange MB, Porte-Agel F (2001) On Monin-Obukhov similarity in the stable atmospheric boundary layer. *Bound Layer Meteorol* 99:225–248
- Panosfsky HA, Dutton JA (1984) *Atmospheric turbulence: Models and methods for engineering applications*. John Wiley Sons, New York
- Pardyjak ER, Monti P, Fernando HJS (2002) Flux Richardson number measurements in stable atmospheric shear flows. *J Fluid Mech* 459:307–316
- Petersen EL, Mortensen NG, Landberg L, Hjstrup J, Frank HP (1998) *Wind power meteorology Part I climate and turbulence*. *Wind Energy* 1(1):2–22

- Prasad KH, Srinivas CV, Satyanarayana ANV, Naidu CV, Baskaran R, Venkatraman B (2015) Formulation of stability-dependent empirical relations for turbulent intensities from surface layer turbulence measurements for dispersion parameterization in a Lagrangian particle dispersion model. *Meteorol Atmos Phys* 127(4):435–450
- Prasad KH, Srinivas CV, Singh AB, Naidu CV, Baskaran R, Venkatraman B (2018) Turbulence characteristics of surface boundary layer over the Kalpakkam tropical coastal station, India. *Meteorol Atmos Phys* 131:1–17
- Rakesh PT, Venkatesan R, Srinivas CV (2013) Formulation of TKE based empirical diffusivity relations from turbulence measurements and incorporation in a Lagrangian particle dispersion model. *Environ Fluid Mech* 13(4):353–369
- Rakesh PT, Venkatesan R, Hedde T, Roubin P, Baskaran R, Venkatraman B (2015) Simulation of radioactive plume gamma dose over a complex terrain using Lagrangian particle dispersion model. *J Environ Radioact* 145:30–39
- Seaman NL, Gaudet BJ, Stauffer DR, Mahrt L, Richardson SJ, Zielonka JR, Wyngaard JC (2012) Numerical prediction of submesoscale flow in the nocturnal stable boundary layer over complex terrain. *Mon Weather Rev* 140(3):956–977
- Skamarock WC, Klemp JB, Dudhia J, Gill DO, Barker DM, Wang W, Powers JG (2005) A description of the advanced research WRF version 2 (No. NCAR/TN-468+STR). National Center For Atmospheric Research Boulder Co Mesoscale and Microscale Meteorology Div
- Smedman A (1988) Observations of a multi-level turbulence structure in a very stable boundary layer. *Bound Layer Meteorol* 44:231–253
- Soler MR, Arasa R, Merino M, Olid M, Ortega S (2011) Modelling local sea-breeze flow and associated dispersion patterns over a coastal area in north-east Spain: a case study. *Bound Layer Meteorol* 140(1):37–56
- Sorbjan Z (1986a) On similarity in the atmospheric boundary layer. *Bound Layer Meteorol* 34:377–397
- Sorbjan Z (1986b) On the vertical distribution of passive species in the atmospheric boundary layer. *Bound Layer Meteorol* 35:73–81
- Sorbjan Z (2006) Local structure of turbulence in stably stratified boundary layers. *J Atmos Sci* 63(5):1526–1537
- Sorbjan Z (2010) Gradient-based scales and similarity laws in the stable boundary layer. *Q J R Meteorol Soc* 136(650):1243–1254
- Srinivas CV, Venkatesan R, Baskaran R, Rajagopal V, Venkatraman B (2012) Regional scale atmospheric dispersion simulation of accidental releases of radionuclide from Fukushima Dai-ichi reactor. *Atmos Environ* 61:66–84
- Srinivas CV, Rakesh PT, Baskaran R, Venkatraman B (2017) Source term assessment using inverse modeling and environmental radiation measurements for nuclear emergency response. *Air Qual Atmos Health* 10(9):1077–1087
- Stohl A, Forster C, Frank A, Seibert P, Wotawa G (2005) The Lagrangian particle dispersion model FLEXPART version 62. *Atmos Chem Phys* 5(9):2461–2474
- Stull RB (1988) An introduction to boundary layer meteorology. Kluwer Academic Publishers, Dordrecht, p 670
- Van de Wiel BJH, Moene AF, Hartogensis OK, De Bruin HAR, Holtslag AAM (2003) Intermittent turbulence in the stable boundary layer over land. Part III: a classification for observations during CASES-99. *J Atmos Sci* 60(20):2509–2522
- van den Berg G (2008) Wind turbine power and sound in relation to atmospheric stability. *Wind Energy* 11(2):151–169
- Wei P, Cheng S, Li J, Su F (2011) Impact of boundary-layer anticyclonic weather system on regional air quality. *Atmos Environ* 45(14):2453–2463
- Wyngaard JC (1975) Modelling the planetary boundary layer-extension to the stable case. *Bound Layer Meteorol* 9:441–460
- Zhu Q, Liu Y, Jia R, Hua S, Shao T, Wang B (2018) A numerical simulation study on the impact of smoke aerosols from Russian forest fires on the air pollution over Asia. *Atmos Environ* 182:263–274
- Zilitinkevich S, Baklanov A (2002) Calculation of the height of the stable boundary layer in practical applications. *Bound Layer Meteorol* 105(3):389–409

Publisher's Note Springer Nature remains neutral with regard to jurisdictional claims in published maps and institutional affiliations.